

3D Creep Analysis of the Leaning Tower of Pisa

05 November 2002

Prof. Dr.-Ing. P.A. Vermeer, Dipl.-Ing. H.P. Neher, Dipl.-Ing. U. Vogler
Institute of Geotechnical Engineering, University of Stuttgart, Germany

Dr. Ir. P.G. Bonnier
PLAXIS B.V. , Delft, The Netherlands

TABLE OF CONTENT

1	Introduction	3
2	Description of Models	4
2.1	Soft-Soil Model with $\phi' = \phi'_{cs}$	4
2.2	Soft-Soil-Creep Model with $\phi' = \phi'_{cs}$	8
3	Selection of Parameters	12
4	3D Finite Element Model	16
4.1	Modelled History of the Leaning Tower of Pisa	16
4.2	Geometry of the 3D Finite Element Model	17
5	Results of Drained Analysis with Soft-Soil Model	21
6	Results of Drained Analysis with Soft-Soil-Creep Model	24
7	Consolidation Analyses	27
7.1	Sequence of Consolidation Analyses with Soft Soil Creep Model	27
7.2	Data from the 3 rd Consolidation Analysis.....	36
7.3	Counterweights, Soil Extraction and Future Creep.....	42
8	Conclusions	45
9	Literature.....	46

3D Creep Analysis of the Leaning Tower of Pisa

05 November 2002

1 Introduction

The aim of this report is to describe a 3D finite element model, which is able to simulate the deformation history of the Leaning Tower of Pisa. This model simulations include the recent rescue operations (applying of counterweight and soil extraction) and also a prediction of the tower behaviour for the coming 100 years. The effort is focused on an analysis which includes creep effects. As a reference calculation, however, an analysis without creep is considered. The described analyses have been ordered by the Consorzio Progetto Torre di Pisa. The Institute of Geotechnical Engineering at the University of Stuttgart, Germany, and PLAXIS BV, Delft, The Netherlands, have been given the assignment by letter of April 27, 2001.

In this report the Soft-Soil model and the Soft-Soil-Creep model, as applied in this study, are explained first. Following this, the selection of parameters for the soil layers is considered on the basis of earlier publications and reports. Furthermore, the 3D finite element model being used is specified. This includes the initial mesh before the beginning of all construction stages and further all specified construction stages of the tower, as well as the recent rescue operations. The tower inclination history and estimated settlements are used for calibration of the model to ensure a reasonable prediction of the future. The results of the 3D finite element analyses are reported in subsequent sections. This report concludes with a summary.

2 Description of Models

In this chapter the two constitutive relations, which are used to describe the behaviour of the clayey sub-layers under the Leaning Tower of Pisa, are explained. The sand layers are modelled with the well-known Mohr-Coulomb model. The latter model is not described in this report.

2.1 Soft-Soil Model with $\phi' = \phi'_{cs}$

Some of the main characteristics of the Soft-Soil model are described through the following features:

- Stress dependent stiffness (logarithmic compression behaviour).
- Distinction between primary loading and unloading-reloading.
- Use of the pre-consolidation stress as a yield stress.
- Failure behaviour according to the Mohr-Coulomb criterion.

In the Soft-Soil model it is assumed that there is a logarithmic relation between the volumetric strain ε_v and the mean effective stress $p' = -(\sigma_1' + \sigma_2' + \sigma_3')/3$ which can be formulated as

$$\varepsilon_v - \varepsilon_{v0} = -\lambda^* \cdot \ln \frac{p'}{p'_0} \quad (\text{virgin isotropic compression}) \quad (1)$$

where ε_{v0} is the initial volumetric strain and p'_0 is the initial mean effective stress. The definition of the natural volumetric strain ε_v is given in Equation 2.

$$\varepsilon_v = \ln \frac{V}{V_0} \quad (2)$$

Herein the initial volume is V_0 and the actual one is V . The parameter λ^* is a modified compression index, which determines the compressibility of the material in primary loading. Note that the classical sign convention of mechanics, which says that extension is positive both for stress and strains, is used. The index λ^* differs from the index λ because the first relates to the volumetric strain ε_v and the second to the void ratio e . When plotting Equation 1 with a logarithmic stress scale one obtains a straight line as shown in Figure 1. During isotropic unloading and reloading a different line is followed which is described by the following equation

$$\varepsilon_v^e - \varepsilon_{v0}^e = -\kappa^* \cdot \ln \frac{p'}{p'_0} \quad (\text{isotropic unloading and reloading}) \quad (3)$$

The parameter κ^* is a modified swelling index, which determines the compressibility of the material in unloading and subsequent reloading. In Equation 3 the soil response during unloading and reloading is assumed to be elastic, which is expressed by the superscript e .

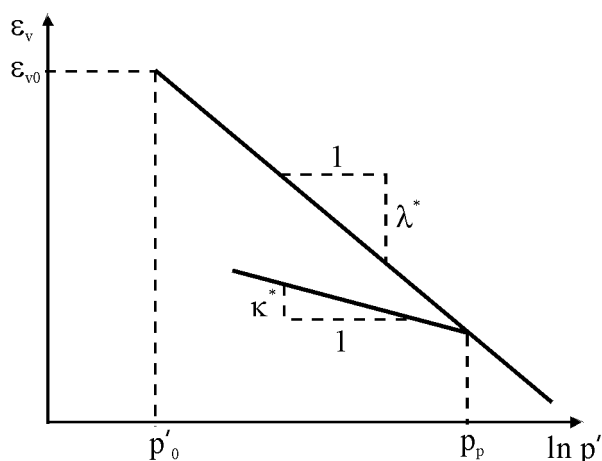


Figure 1: Logarithmic relation between volumetric strain and mean stress

The elastic behaviour is described by Hooke's law of elasticity. Equation 3 implies the following linear stress dependency of the tangent bulk modulus

$$K_{ur} \equiv \frac{E_{ur}}{3(1-2\nu_{ur})} = \frac{p'}{\kappa^*} \quad (4)$$

The subscripts *ur* is used to denote that the parameters relate to unloading and reloading.

Yield function for triaxial stress state ($\sigma_2' = \sigma_3'$)

For a triaxial state of stress the yield function of the Soft-Soil model is defined as

$$f = \bar{f} - p_p \quad (5)$$

where \bar{f} is a function of the stress state (p' , q) and the pre-consolidation stress p_p is a function of plastic strain:

$$\bar{f} = \frac{q^2}{M^2 p'} + p' \quad \text{and} \quad p_p = p_{p0} \exp\left(\frac{-\varepsilon_v^p}{\lambda^* - \kappa^*}\right) \quad (6)$$

$$\text{with } M = \frac{6 \sin \varphi_{cs}}{3 - \sin \varphi_{cs}} \quad \text{and} \quad q = |\sigma_1' - \sigma_3'|$$

The yield function f describes an ellipse in p' - q -plane as illustrated in Figure 2. The parameter M in Equation 6 determines the height of the ellipse. In the p' - q -plane the tops of all ellipses are located on a line with inclination M . In the modified Cam-Clay model (Burland 1965, 1967) the M -line is referred to the Critical State Line and represents stress states at post peak failure. In the Soft-Soil model failure is not necessarily connected to critical state, but in this study the critical state angle is used as a failure state; softening is not considered. The isotropic pre-consolidation stress p_p determines the magnitude of the ellipse.

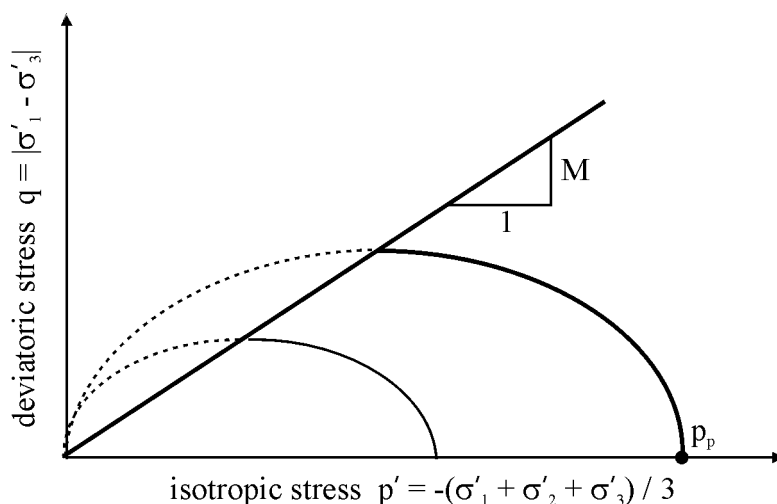


Figure 2: Yield surface of the Soft-Soil model in p' - q -plane

The value of p_p is determined by volumetric plastic straining and follows from the hardening relation as formulated in Equation 6. The value p_{p0} can be regarded as the initial value of the pre-consolidation stress. According to Equation 6 the initial volumetric plastic strain is assumed to be zero.

The yield contour as shown by the bold lines in Figure 2 is the boundary of the elastic stress area. The failure line is fixed, but the cap may increase due to primary compression. Stress paths within this boundary give only elastic strain increments, whereas stress paths, that tend to cross the boundary generally give both elastic and plastic strain increments.

Parameters in the Soft-Soil model $\varphi' = \varphi'_{cs}$

λ^*	:	Modified compression index	[-]
κ^*	:	Modified swelling index	[-]
φ'_{cs}	:	critical state friction angle	[°]
ν_{ur}	:	Poisson's ratio for unloading/reloading	[-]

Apart from isotropic compression tests the parameters κ^* and λ^* can be obtained from one-dimensional compression tests. Here the relationship exists with the traditional indices for one-dimensional compression and unloading/reloading, C_c and C_s .

$$\lambda^* = \frac{C_c}{2.3(1+e)} \quad \text{and} \quad \kappa^* \approx \frac{3}{2.3} \cdot \frac{1-v_{ur}}{1+v_{ur}} \cdot \frac{C_s}{(1+e)} \quad (7)$$

Another relationship exists with the Cam-Clay parameters (see also Brinkgreve & Vermeer, 1998/2001).

$$\lambda^* = \frac{\lambda}{1+e} \quad \text{and} \quad \kappa^* = \frac{\kappa}{1+e} \quad (8)$$

2.2 Soft-Soil-Creep Model with $\phi = \phi_{cs}$

Some of the main characteristics of the Soft-Soil-Creep model are described through the following features:

- Stress dependent stiffness (logarithmic compression behaviour).
- Distinction between primary loading and unloading-reloading.
- Secondary (time-dependent) compression
- Use of pre-consolidation stress as a yield stress.
- Failure behaviour according to the Mohr-Coulomb criterion.

The Soft-Soil-Creep model is an extension of the Soft-Soil model, by taking account of creep. The only additional parameter is a modified creep index μ^* .

Basics of one-dimensional creep

The secondary compression is described as

$$\varepsilon = \varepsilon_c - \mu^* \cdot \ln \frac{\tau_c + t'}{\tau_c} \quad (9)$$

where ε is the logarithmic strain defined as

$$\varepsilon = \ln \frac{V}{V_0} = \ln \frac{1+e}{1+e_0} \quad (10)$$

The parameters μ^* and τ_c can be evaluated from experimental data by using ideas as developed by Janbu (1969). Both the traditional way, being indicated in Figure 3a, as well as the Janbu method of Figure 3b can be used to determine the parameter μ^* from an oedometer test, in which the load is kept constant. The use of the Janbu method is attractive, because both μ^* and τ_c result directly when fitting a straight line through the data. In Janbu's representation of Figure 3b τ_c is the intercept with the (non-logarithmic) time axis of the straight creep line. The deviation from a linear relation for $t < \tau_c$ is due to consolidation. Please note that in the present model τ_c is not needed.

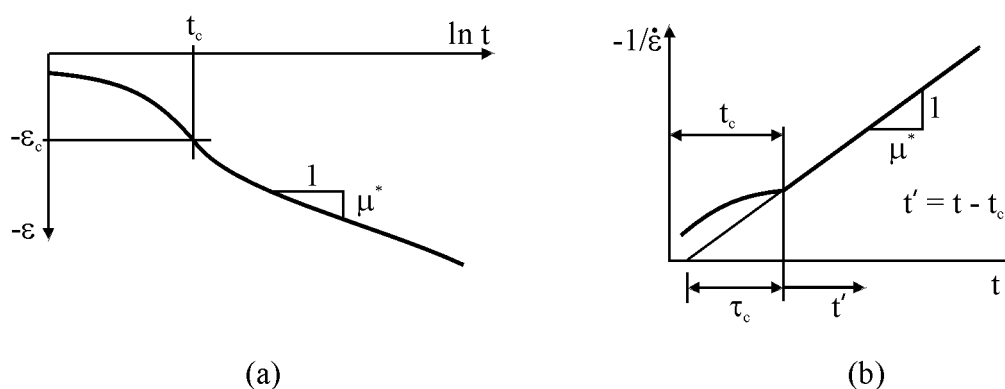


Figure 3: Consolidation and creep behaviour in standard oedometer test

3D model

The invariants p' and q are used to define a new stress measure named p^{eq}

$$p^{eq} = p' + \frac{q^2}{M^2 p'} \quad (11)$$

Please note that in the context of the Soft-Soil-Creep model an isotropic pre-consolidation stress is denoted as p_p^{eq} whereas the notation p_p was used to explain the Soft-Soil model. In Figure 4 it is shown that the stress measure p^{eq} is constant on ellipses in p' - q -plane. Like in the Soft-Soil model, the Mohr-Coulomb failure criterion is used with $\phi' = \phi'_{CS}$.

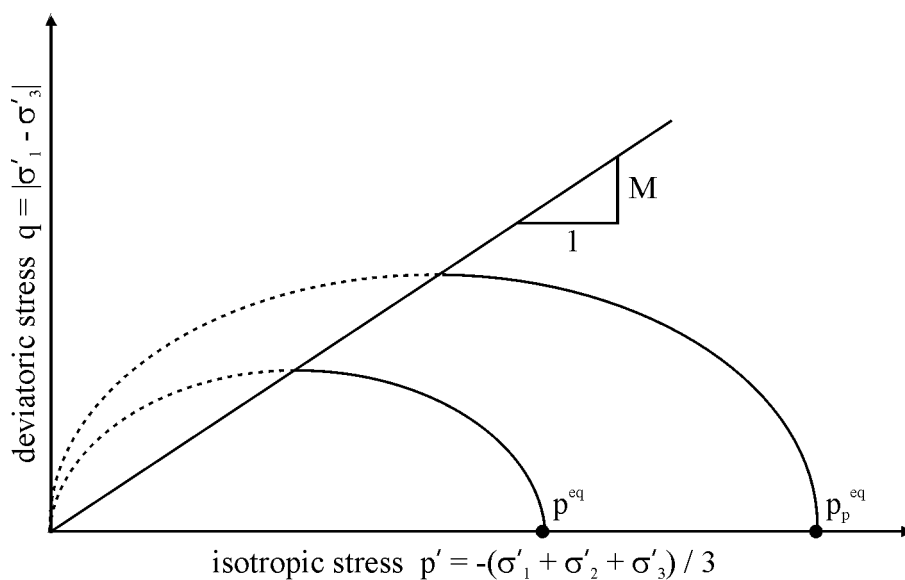


Figure 4: Diagram of p^{eq} -ellipses in a p' - q -plane

By introducing the material parameters κ^* , λ^* and μ^* the volumetric creep strain can be obtained from the following equation

$$-\dot{\varepsilon}_v^c = \frac{\mu^*}{\tau} \cdot \left(\frac{p^{eq}}{p_p^{eq}} \right)^{\frac{\lambda^* - \kappa^*}{\mu^*}} \quad \text{with} \quad p_p^{eq} = p_{p0}^{eq} \exp\left(\frac{-\varepsilon_v^c}{\lambda^* - \kappa^*} \right) \quad (12)$$

Using Hooke's law for the elastic strain and a flow rule for the creep strain the total strains are defined as

$$\dot{\varepsilon} = \mathbf{D}^{-1} \dot{\sigma}' + \frac{\dot{\varepsilon}_v^c}{\alpha} \cdot \frac{\partial p^{eq}}{\partial \sigma'} = \mathbf{D}^{-1} \dot{\sigma}' - \frac{1}{\alpha} \cdot \frac{\mu^*}{\tau} \cdot \left(\frac{p^{eq}}{p_p^{eq}} \right)^{\frac{\lambda^* - \kappa^*}{\mu^*}} \frac{\partial p^{eq}}{\partial \sigma'} \quad (13)$$

with $\alpha = \frac{\partial p^{eq}}{\partial p'} = 1 - \frac{q^2}{M^2 p^2}$ and $\tau = 1 \text{ day}$

where \mathbf{D} is the elasticity matrix. It involves the modified swelling index κ^* and the Poisson ratio ν_{ur} as expressed by Equation 4. The stress measure p^{eq} is also used as a plastic potential function.

Parameters in the Soft-Soil-Creep model

λ^*	:	Modified compression index	[-]
κ^*	:	Modified swelling index	[-]
μ^*	:	Modified creep index	[-]
φ'_{cs}	:	Friction angle	[°]
ν_{ur}	:	Poisson's ratio for unloading/reloading	[-]

Modified swelling index, modified compression index and modified creep index

The modified swelling index and the modified compression index can be determined as explained in section 2.1. The parameter μ^* can be obtained by measuring the volumetric strain on the long term and plotting it against the natural logarithm of time (see Figure 3).

Apart from isotropic compression tests the parameters κ^* , λ^* and μ^* can be obtained from one-dimensional compression tests. This is possible by using the relationships of Equations 7 and 8. Moreover the creep index C_α can be related to the modified creep index μ^* by

$$\mu^* = \frac{C_\alpha}{2.3(1+e)} \quad (14)$$

For a more detailed description (especially the transition from 1D to 3D stress states) of the Soft-Soil-Creep model, the reader is referred to Vermeer and Neher (1999).

3 Selection of Parameters

The sand layers are modelled by using the Mohr Coulomb model. For the clay layers two different models are used; the Soft-Soil model and the Soft-Soil-Creep model. Both are implemented in the PLAXIS FE-code that is used for the present 3D calculations. The parameters required for the models are already mentioned in the previous section. The division of the subsoil into two horizons A and B and their respective sub-layers as well as the position of the sub-layers are adopted according to Potts (1993) and Calabresi (1996). In the following, the vertical position of the sub-layers is given with respect to the sea level.

Horizon A

MG	+3.0 m to 0.0 m.	top soil and man made ground
A1	+0.0 m to 5.2 m	loose to very loose yellow sandy silt to clayey silt without stratification
A2	-5.2 m to -7.4 m	uniform grey sand with interbedded clay layers, broken fossils – upper sand

Horizon B

B1	-7.4 m to -10.9 m	highly plastic grey clay with fossils
B2	-10.9 m to -12.9 m	medium plastic grey clay with fossils
B3	-12.9 m to -17.8 m	highly plastic grey clay with fossils
B4	-17.8 m to -19.0 m	dark grey organic clay
B5	-19.0 m to -22.0 m	blue grey to yellow silty clay with calcareous nodules
B6	-22.0 m to -24.4 m	grey, sometimes yellow, sand and silty sand – intermediated sand
B7	-24.4 m to -29.0 m	medium to highly plastic clay with fossils and thin sand layers in the upper part
B8	-29.0 m to -30.4 m	grey clay with frequent thin sand lenses
B9	-30.4 m to -34.4 m	blue grey silty clay with yellow zones, calcareous nodules, some dark organic clay at centre
B10	-34.4 m to -37.0 m	grey clay with yellow zones, fossils in the lower part

These layers are underbedded by a stiff sand called C1 in horizon C that can be treated as a natural boundary. More detailed information about the subsoil in Pisa is given by Calabresi (1996).

The parameter λ^* is calculated using Equation 7, with C_c and e -values as indicated in Figure 15. For the parameter κ^* a fixed ratio of $\lambda^*/\kappa^* = 10$ is adopted. This is done in accordance to Potts (1993). The ratio $\lambda^*/\mu^* = 30$ is set using our experience in this field as well as cross-checking it with the C_α -values from Calabresi (1996) and data by Mesri & Choi (1985). Calabresi finds ratios of about 40, whereas Mesri & Choi suggest for inorganic soft clays $C_\alpha/C_c = 0.04 \pm 0.01$, which corresponds to $\lambda^*/\mu^* = 20 - 33$. Hence the value of 30 is more or less in between the data by Calabresi and general data by Mesri & Choi.

Table 1: Soil parameters for the Soft Soil (SS) and the Soft Soil Creep (SSC) model.

layer	γ [kN/m ³]	λ^* [-]	κ^* [-]	μ^* [-]	v_{ur} [-]	ϕ'_{cs} [°]	k [10 ⁻¹⁰ m/s]
A1N	19.1	0.04	0.004	0.0013	0.15	34.0	10000
A1S	19.1	0.07	0.007	0.0023	0.15	34.0	10
B1	17.3	0.15	0.015	0.005	0.15	26.0	5
B2	17.8	0.12	0.012	0.004	0.15	26.0	5
B3	16.7	0.15	0.015	0.005	0.15	26.0	5
B4/B5	20.0	0.07	0.007	0.0023	0.15	28.0	2
B7a	19.6	0.1	0.01	0.0033	0.15	27.0	5
B7b	17.8	0.12	0.012	0.004	0.15	27.0	5
B8/B9/B10	19.0	0.1	0.01	0.0033	0.15	25.0	3

Table 2: Soil parameters for the Mohr-Coulomb model.

layer	γ [kN/m ³]	E [kPa]	ν [-]	ϕ' [°]	c' [kPa]	ψ [°]	k [10 ⁻¹⁰ m/s]
MG	18.0	8700	0.33	34.0	20.0	0.0	10000
A2	18.2	13700	0.33	34.0	0.0	0.0	10000
B6	19.1	11600	0.33	34.0	0.0	0.0	10000

The division of the A1 layer into a North (A1N) and a South (A1S) part is done to trigger the inclination of the tower. It should be noted that this is the only triggering in the model.

For the tower itself linear elasticity is assumed and related parameters are given in Table 3. The stiffness is assumed to be the same over the entire tower. The high stiffness is chosen to avoid any self-deformation of the tower. For the sake of convenience the diameter of the tower is kept the same over the total height. The

weight has been changed with respect to the real situation in order to get the appropriate vertical load as well as the correct turning moment.

Table 3: Model parameters for the tower

layer	γ [kN/m ³]	E [kPa]	ν [-]
Foundation	24.0	$5 \cdot 10^{+7}$	0.0
1 st floor	10.9	$5 \cdot 10^{+7}$	0.0
2 nd to 6 th floor	7.5	$5 \cdot 10^{+7}$	0.0
7 th floor	6.1	$5 \cdot 10^{+7}$	0.0
bell chamber	2.9	$5 \cdot 10^{+7}$	0.0

4 3D Finite Element Model

4.1 Modelled History of the Leaning Tower of Pisa

1173 to 1178	Construction of the foundations and the first four levels (reaching the height of 29 m)
1178 to 1272	Interruption of construction
1272 to 1278	Construction of the tower to the eight level (reaching the height of 51 m)
1278 to 1360	Interruption of construction
1360 to 1370	The Tower was completed with the bell chamber to its final height of 58 m
1838 / 1839	Execution of an annular excavation (Catino) to uncover the lowest part of the Tower, which had previously been buried
May 1993	A pre-stressed concrete ring (100 t) was constructed around the base of the tower at plinth level
July 1993	Application of a counterweight of 600 t in four phases with a pause between each phase to give time for response of the tower
January 1994	Placing of the last ingot
February 1999	First soil extraction under the north side of the tower.
February 2000	Second soil extraction

The water proofing of the Catino 1933 to 1935 and the lowering of the ground water head in deeper layers from 1970 to 1975 are not modelled, because it is not considered of much interest to the history of the tower.

In the first phase of construction the foundation is built and after that the tower is constructed successively by adding floors up to a height of 29 m. In the second phase the tower is increased to the seventh floor up to a total height of 51 m. In the third phase the tower is completed with the bell chamber and the final height of 58 m is reached.

After construction of the tower a ditch, the so-called Catino, was dug in 1838. The Catino is modelled around the entire tower with an assumed width of 1.2 m and a depth of 2 m in the south and 1 m in the north. The ditch made it possible to enter the portal of the tower easily again, but the Catino increased the ratio of tilting.

The mounting of counterweights in 1993 is simulated by a load of 7 MN on the north side of the foundation. The centre of the load is on the symmetry line of the tower at a distance of 7.5 m out of the tower axis.

Soil extraction is simulated by reducing the volume of elements at a depth of 4.5 m under the foundation on the north side. This is done in two steps; the first step (1999) by excavating 6.8 m³ and the full excavation in 2000 by excavating additionally 18.2 m³. Excavation was modelled using shrinking elements. Soil is taken out directly under the tower and the Catino as indicated in Figure 26.

4.2 Geometry of the 3D Finite Element Model

Three-dimensional finite element calculations are done by considering the effects of large strains on the basis of the updated Lagrange method. Geometric non-linearity is thus considered. To reduce computer capacity calculations are carried out in a half symmetric model with north-south direction as symmetric axis. The 3D mesh is bounded by the lower sand at 40 m under the terrain surface. This sand is relatively stiff

and represented by a fully fixed bottom boundary. Vertical boundaries are placed at 50 m distance from the centre of the tower such that the sub-soil model is one symmetric half of a square block. At the vertical boundaries, displacements are only fixed in normal direction (roller conditions).

The foundation is modelled as a circular footing with a diameter of 19.6 m and an integrated depth of 3 m into the man made ground. To simplify the model, the foundation is not modelled as a ring with an inner diameter of 4.5 m, but as a full circle. The use of a real ring foundation would reduce the area of the foundation by 5.3%, but the finite element mesh would be much more complex.

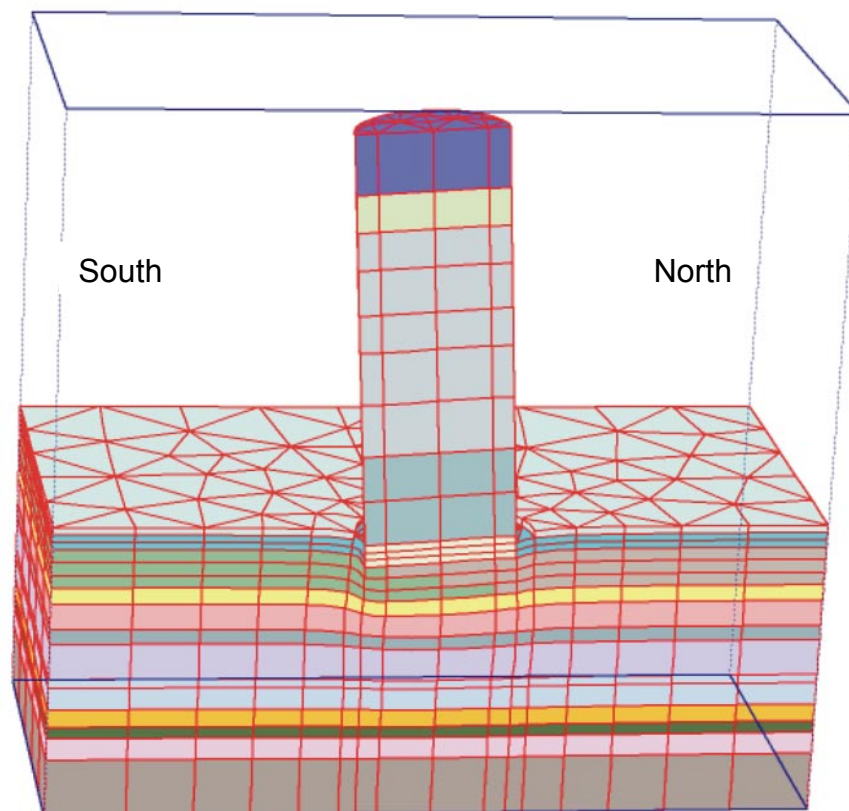


Figure 5: Deformed Mesh

The FE-mesh, see Figure 5, consists of 4400 elements, 12789 nodes and 4 degrees of freedom per node. The tower is modelled in 9 parts for simulating the different loading stages. The subsoil is divided into 12 sub-layers to simulate the varying soil properties and the different states of over-consolidation.

In the mesh 15-noded prismatic elements are used in combination with 6 Gaussian integration points. The tower itself is also simulated by 15-noded prismatic elements (with linear elastic behaviour). It consists of a cylinder with a diameter of 19.6 meters over the whole length. This is done again to simplify the geometry as much as possible. The weights of the different parts (floors) are recalculated in accordance to their new geometry so that the turning moment and the vertical load agree with reality. Distinctions have been made between foundation, first floor, second to sixth floor, seventh floor and bell chamber. The modelled tower has a weight of 145 MN and the centre of gravity of the full tower is located at a height of 22.34 m above the foundation bottom line.

The varying parameters of the triggering silt layer (A1) are simulated by using two different sets of parameters (κ^* , λ^* and μ^* values) and grading them over three steps from north to south. The selected pre-consolidation stress state is given in Figure 6 in comparison to data collected by Calabresi (1996).

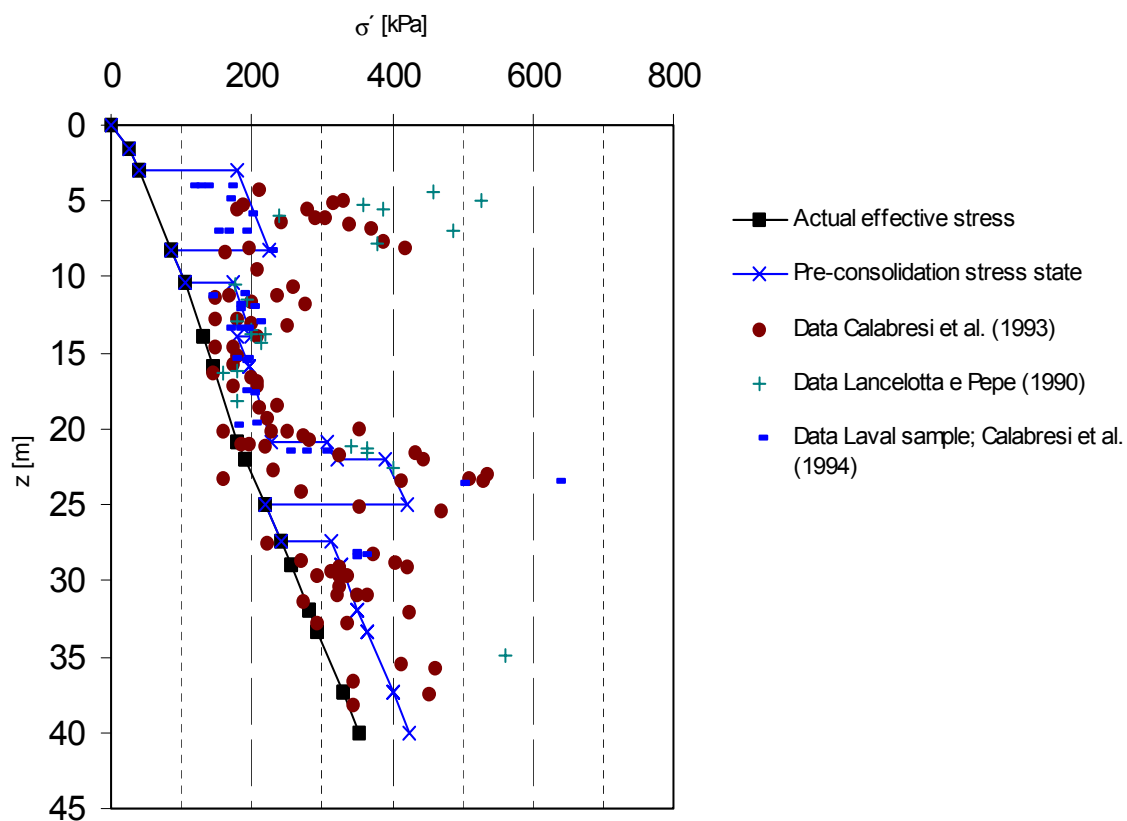


Figure 6: Pre-consolidation stress state

5 Results of Drained Analysis with Soft-Soil Model

As mentioned in Section 2.1 the so-called Soft-Soil model may be applied with a relatively flat yield cap such that it virtually coincides to the Modified Cam-Clay model. In fact this option was chosen by defining $\phi' = \phi'_{cs}$. For large deformations, some differences remain as the Soft-Soil model uses for instance $\lambda^* = \lambda/(1+e)$ as a constant and not λ . Hence both models will behave slightly different when considering large variations of e . Moreover the logarithmic strain is used, which will differ from the engineering strain in the case of large strains.

Computed inclinations of the tower are shown in Figure 7. Considering results from a calculation that does not include any time effects, neither due to consolidation nor to creep, one observes instantaneous responses to all phases of construction, including the excavation of the Catino. Finally this yields an inclination of about 1° , which is well below the measured inclination of 5.5° . After the second phase of construction, the present analysis yields inclinations that are well below an estimate of the Associazione Geotechnica Italiana (AGI) made in 1991. Apparently drained, non-creep analyses need much more triggering in order to simulate a substantial inclination. Here, it is recalled that we triggered the inclination by taking slightly different compression indices within the silt layer (A1) directly underneath the foundation as indicated in Table 1.

The very first analysis (drained and no creep) gives average settlements that agree quite well with an estimation by AGI (1991) as can be seen in Figure 8. The latter estimate is apparently based on a non-tilting tower, as this would explain the coincidence with our computational results. Here it should be noted that Jamiolkowski (1999) has estimated an average settlement of about 3 m on the bases of measurements, including data from neighbouring buildings.

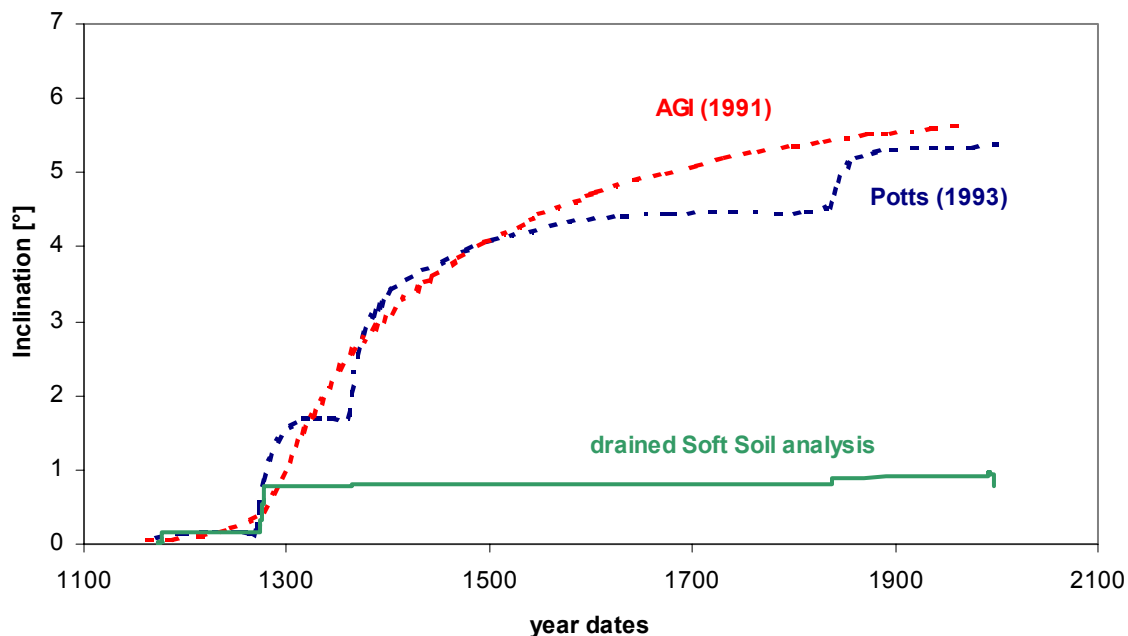


Figure 7: Calculated inclinations with Soft-Soil model (SS) in comparison to AGI and Potts

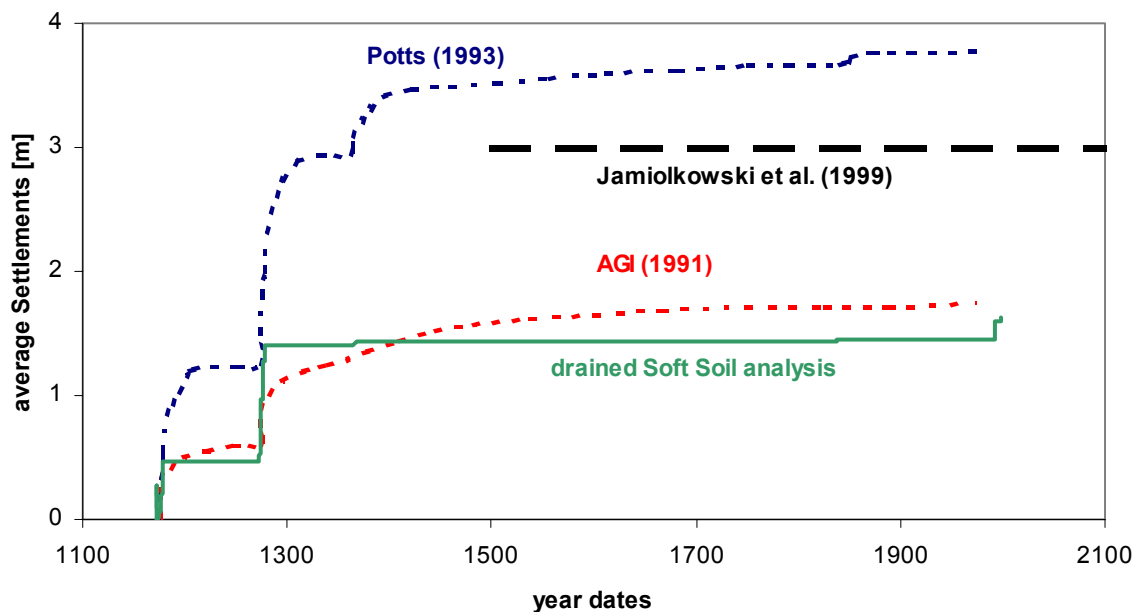


Figure 8: Calculated average settlements in comparison to AGI and Potts

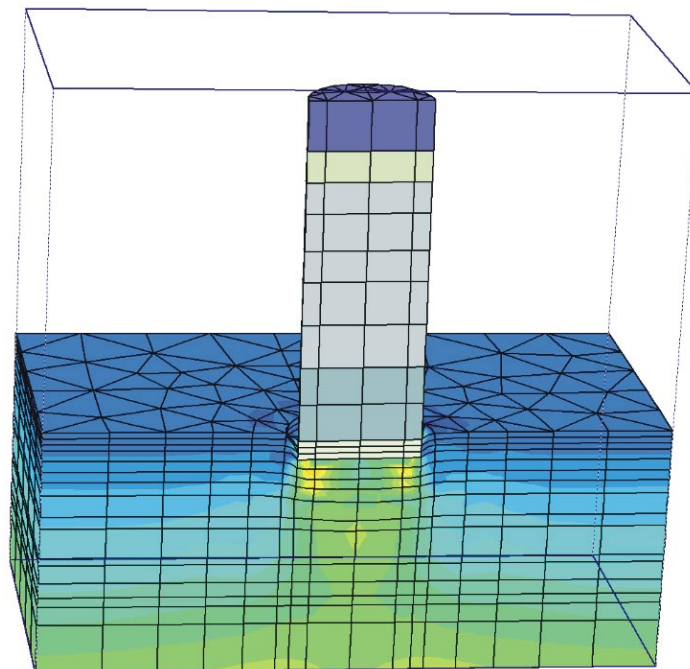


Figure 9: Effective vertical stress using the Soft-Soil model

The relatively small computed inclination of the tower is reflected in Figure 9. This figure shows the intensity of vertical effective stresses after excavation of the Catino. The yellow zones indicate stress levels of 733 kPa at an average foundation pressure of about 500 kPa. The relatively small difference between these values is in line with the relatively small inclination of only one degree.

6 Results of Drained Analysis with Soft-Soil-Creep Model

On using exactly the same input data, the Soft-Soil-Creep model gives much better results than the Soft-Soil model. This is first of all observed in Figure 10 for the inclination of the tower. In contrast to the elastoplastic analysis the present elastoviscoplastic analysis approaches the AGI-curve reasonably well and similar the computational results by Potts (1993). The curve is found to depend on the amount of triggering in the silt layer (A1) directly under the foundation. This silt layer has an average compression index of $\lambda^* = 0.055$; the sandy north side is given the value of 0.04 and the clayey south side is assigned the value 0.07, as indicated in Table 1. Smaller differences between both sides will lead to a somewhat smaller inclination of the tower and vice versus.

It would seem that the impact of the Catino excavation on the inclination relates to some extent to the non-uniform depth of this ditch around the tower. Indeed, the southern part obtains a depth of 2 m and the northern part only 1 m. Hence supporting shear stresses were especially removed on the passive side where the wall friction tends to be large.

Both the loading of the north side by lead ingots and the soil extraction have been simulated numerically. In Figure 10 the effects of the counterweight loading can hardly be observed, but the soil extraction is seen to cause an inclination reduction of about 0.5 degrees. In addition the soil extraction reduces the future rate of further tilting significantly. Considering present computational data, it would seem to last some 500 years before the inclination is back to its past peak value. However, we consider preliminary results of a drained analysis and the model has not yet been sufficiently calibrated.

Some lack of model calibration is also observed when considering the computed time-settlement curve in Figure 11. It is seen that the computed average settlement is well

beyond the most realistic estimate of about 3 m by Jamiolkowski (1999). This testifies the need for further calibration of the present model.

Figure 12 shows data on the mobilisation of the shear strength in the various soil layers. Red zones indicate a fully plastic state of stress where stresses satisfy the Mohr-Coulomb criterion. This typically happens in the relatively stiff sand layers, where a few percent of strain will already imply a plastic state of stress. Fully plastified zones are also observed around the tower in the fill and the underlain silt layer. We consider this realistic for the active and passive side of the silt layer, but not for the large zone of the fill around the tower. The large plastic fill zone is most definitely due to the use of an extremely high Young's modulus of $E = 8700$ kPa (see Table 2). This indicates again the need for further calibration of the present model.

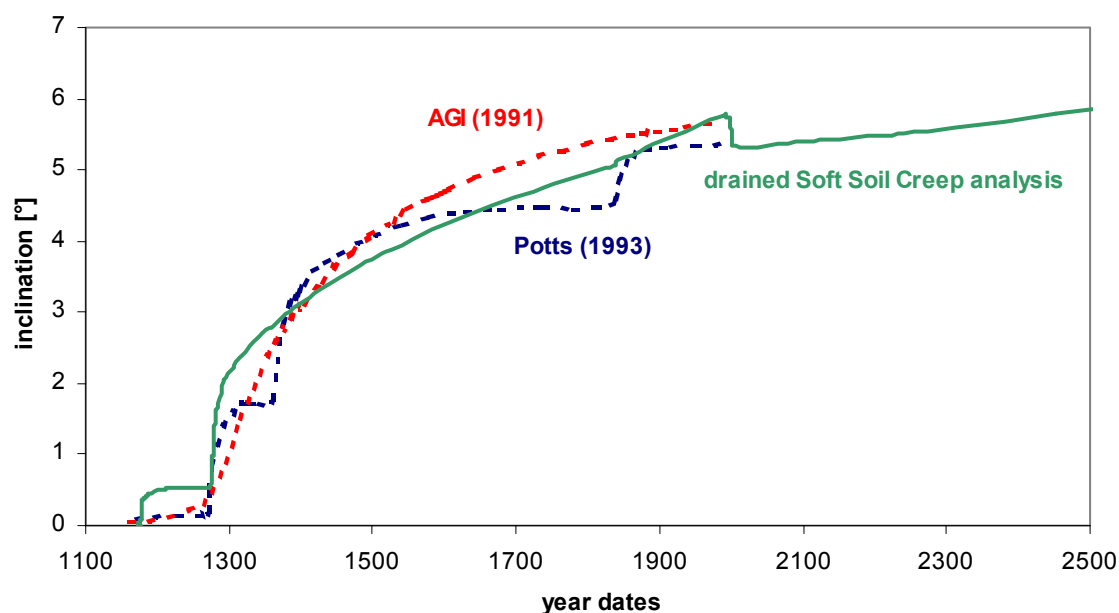


Figure 10: Calculated inclinations with Soft-Soil-Creep model (SSC) in comparison to AGI and Potts

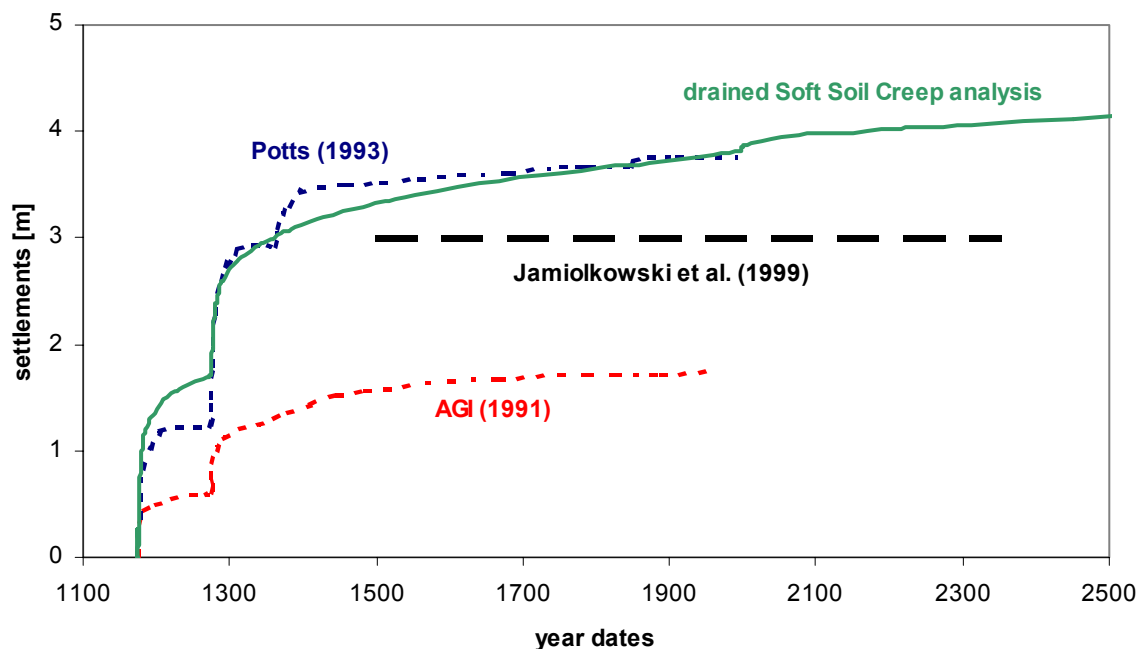


Figure 11: Calculated average settlements from drained Soft-Soil-Creep analysis in comparison to AGI and Potts

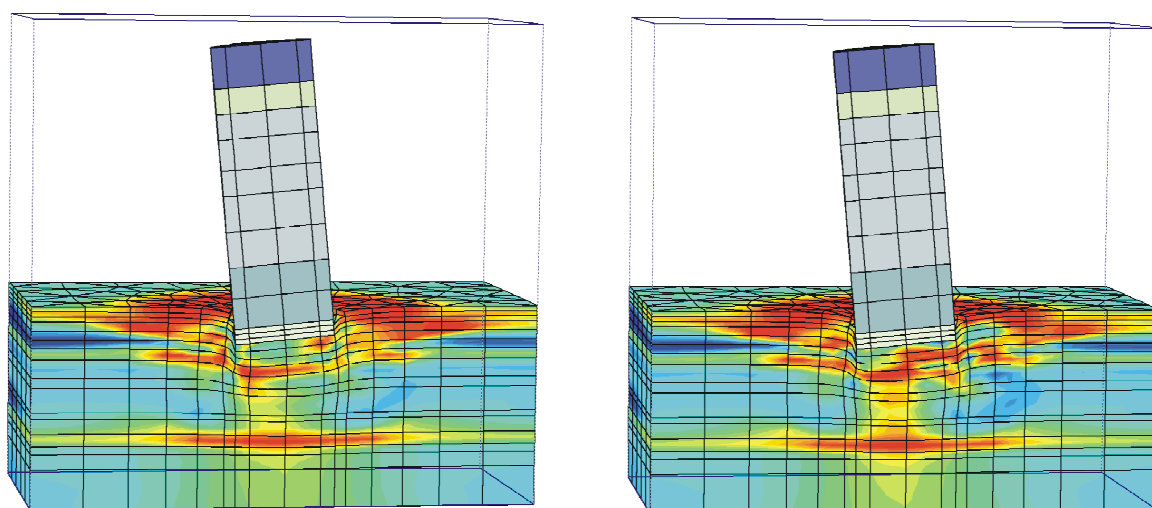


Figure 12: Relative shear strength shadings before (left) and after (right) soil extraction. Red colour is used to indicate zones with full mobilisation of shear strength.

7 Consolidation Analyses

7.1 Sequence of Consolidation Analyses with Soft Soil Creep

Model

In this section results of three-dimensional consolidation analyses are described. All analyses were carried out using the Soft-Soil-Creep model with fully coupled consolidation, so that time effects due to creep as well as due to drainage of pore water are fully included. Moreover the effects of geometric non-linearity are fully included by using the updated Lagrange formulation for large deformations. As for the drained analyses of previous sections, the finite element mesh of Figure 5 will be used.

First consolidation analysis

For the first consolidation analysis we used the soil parameters of Tables 1 and 2. However the triggering of the tilting was slightly changed. Following Potts (1993), we assumed the low permeability coefficient of $k = 10^{-9}$ m/s for the south side of the silt layer (A1) and the relatively high permeability of $k = 10^{-4}$ m/s for the north side of this layer. Further triggering of tilting was achieved by the use of different values of the soil indices.

$$\text{northern silt:} \quad \lambda^* = 0.045 \quad \kappa^* = \lambda^*/10 = 0.0045 \quad \mu^* = \lambda^*/30 = 0.0015$$

$$\text{southern silt:} \quad \lambda^* = 0.065 \quad \kappa^* = \lambda^*/10 = 0.0065 \quad \mu^* = \lambda^*/30 = 0.00217$$

Please note that previous drained analyses were carried out for $\lambda^*_{north} = 0.04$ and $\lambda^*_{south} = 0.07$, so that we effectively reduced the amount of stiffness triggering. This was done because the “non-symmetric” permeability was also expected to contribute to the triggering of tilting. All other soil parameters are as indicated in Tables 3 and 4 and pre-consolidation pressures were taken according Calabresi (1996), as also indicated in

Figure 6. Both the time-settlement curve and the time-inclination curve as resulted from the first consolidation analysis are shown in Figure 14.

Similar to the drained analyses the first consolidation analysis gives large average settlements of about 4 m, which are well beyond the estimated one. We consider the estimate of 3 m most realistic and decided to use this value for calibration of the model.

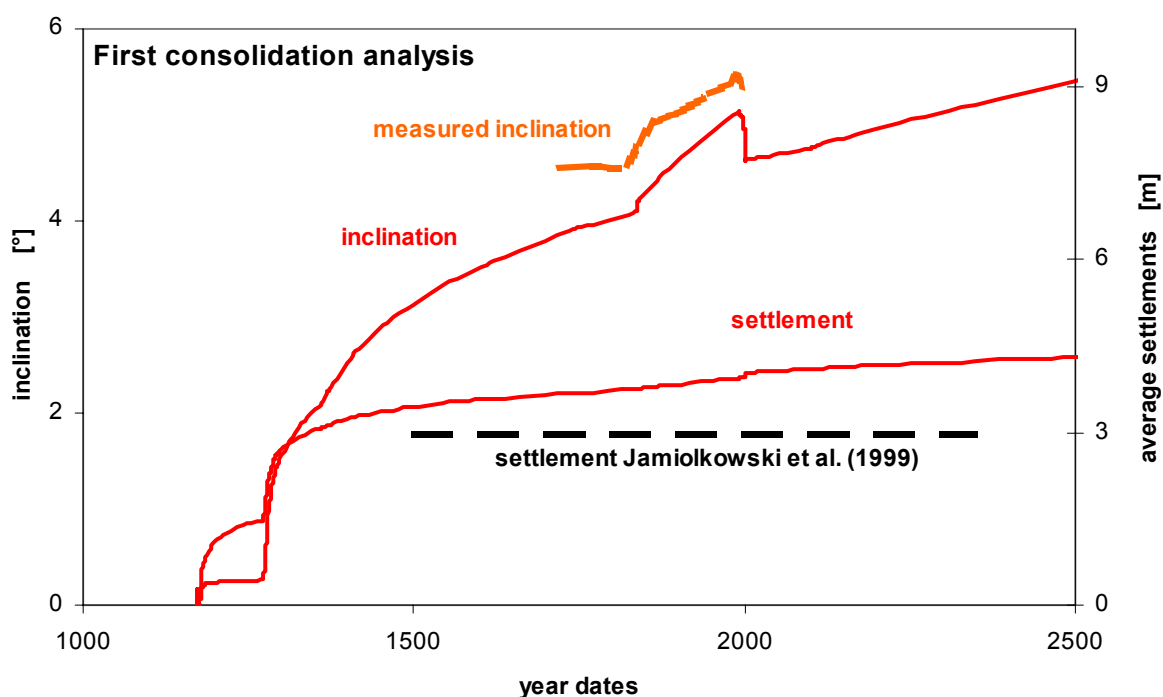


Figure 14: Computational result from first consolidation analysis.

Second consolidation analysis

In order to obtain numerically an average settlement of about 3 m, the stiffnesses of the clay layers were increased, i.e. the compression indices were decreased. The new values are indicated in Table 4. Here it should be noted that all new values are still in the range of existing data from laboratory tests. This is nicely shown in Figure 15, where the new values for λ^* are used to compute $C_c = 2.3 \cdot \lambda^* \cdot (1+e)$. The new values are represented by blue lines and the values for first analyses are indicated in red.

Considering Figure 16 it would seem that we overestimate the C_{α} -values. On the other hand, there is considerable evidence on the ratio of C_{α}/C_c that suggest that our ratio of 0.033 is realistic. Mesri and Choi (1985) obtained for many inorganic soft clays ratios of about 0.04, whereas we use a lower value of 0.033. Hence this would suggest that our C_{α} -values are conservative. We see two possible reasons for the discrepancy between our C_{α} -values and the data in Figure 16. Firstly, the e -values, as listed in Figure 15, that we assumed to compute $C_{\alpha} = 2.3 \cdot \mu^* \cdot (1+e)$, may be somewhat too large. Secondly, it is possible that the laboratory tests have produced somewhat too low C_{α} -values, due to the use of consolidation stresses which were only 50 percent beyond the initial pre-consolidation stress.

Another non-realistic feature of the first consolidation analysis is the relative large increase of the inclination due to the excavation of the Catino. As the Catino excavation happens to be completely done inside the man made fill, it can be concluded that the stiffness of this layer is significantly overestimated. In fact, we did not pay much attention to this layer as we did not immediately recognise its supporting effect. Indeed, the drained analysis showed already a too stiff effect, but not as large as in the first consolidation analysis. Therefore it was decided to decrease the effective cohesion of the fill from 20 kPa down to a more realistic value of 12 kPa and its Young's modulus was reduced down to 1000 kPa.

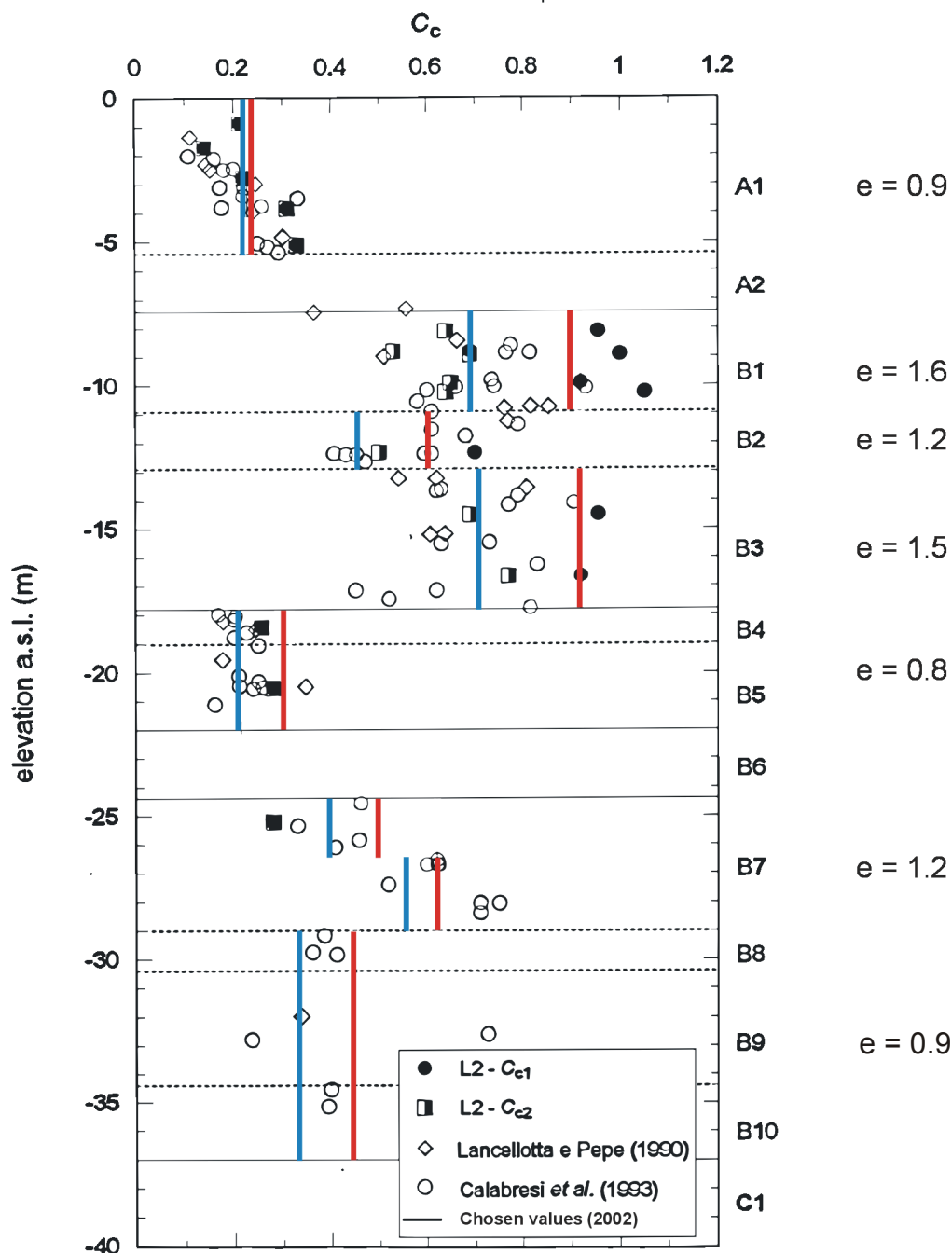


Figure 15: Laboratory data for compression index C_c by Calabresi (1996) in comparison to used ones in the first consolidation analysis (red lines). Blue lines indicate the parameters of all later consolidation analyses.

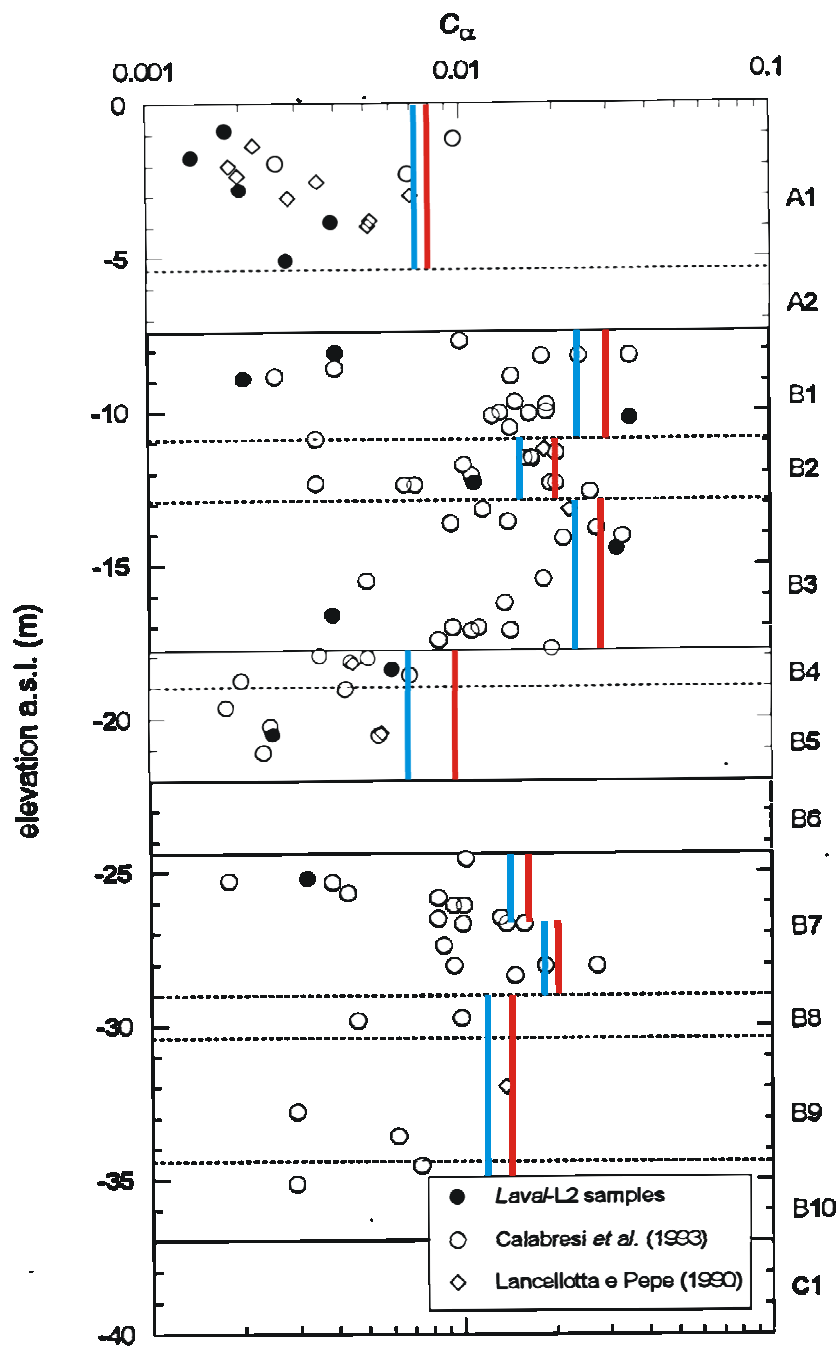


Figure 16: Laboratory data for creep indices C_α by Calabresi (1996) in comparison to used ones. Red indicates the parameters of the first consolidation analysis and blue indicates the parameters of all later consolidation analyses.

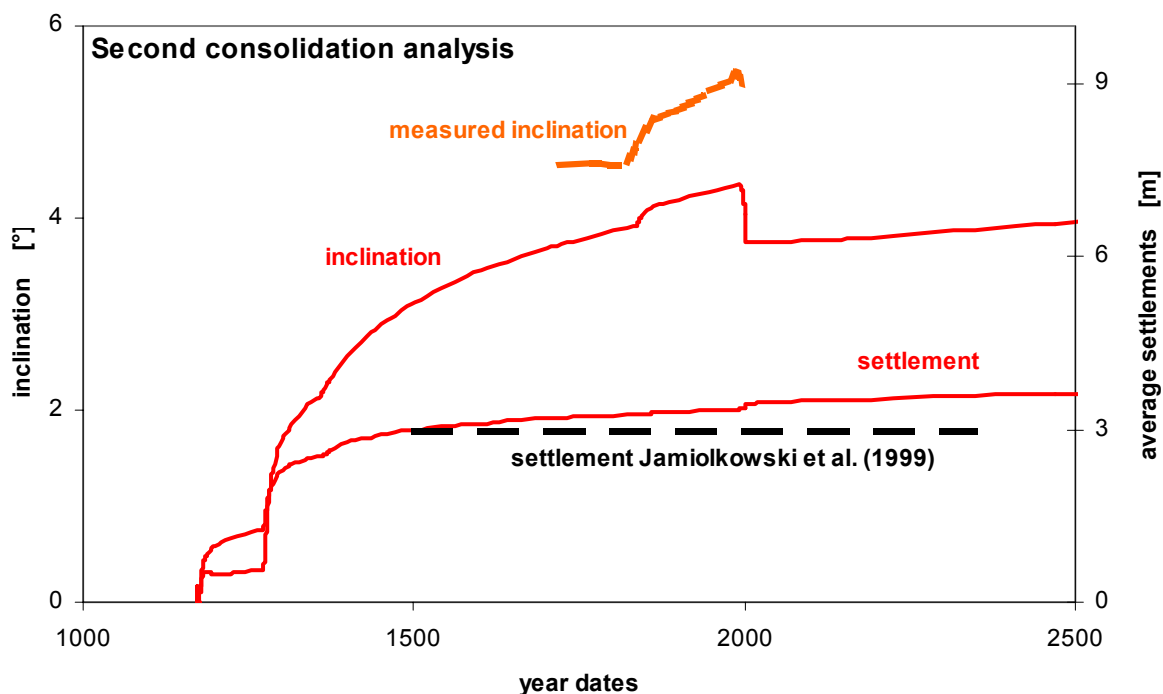


Figure 17: Computational result from second consolidation analysis.

Third consolidation analysis

The second consolidation analysis appears to give a highly realistic average settlement, but a somewhat low inclination, as can be seen in Figure 17. In order to improve the computed inclination, the stiffness of the man made fill was reconsidered. Additionally computations with a Young's modulus of $E = 750$ kPa (not depicted in Figure 18) and $E = 500$ kPa were done. Results as presented in Figure 18 show that the most realistic inclinations are obtained for $E = 500$ kPa.

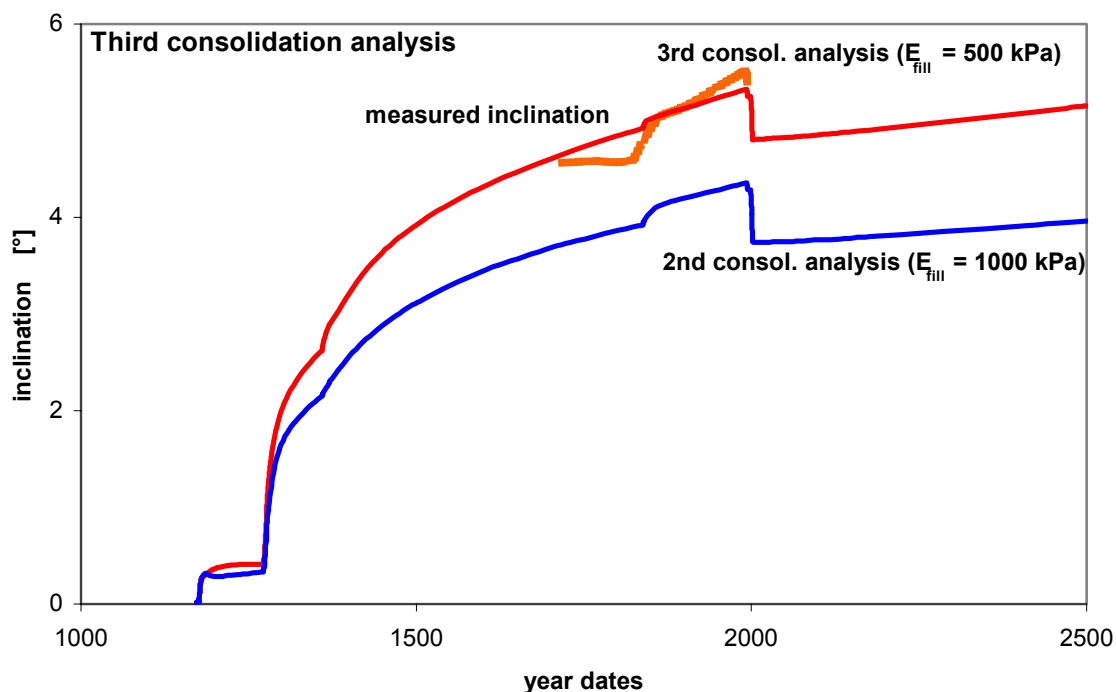


Figure 18: Influence of top layer stiffness on inclination. Stiffnesses of $E_{fill} = 1000$ kPa for the second and $E_{fill} = 500$ kPa for the third consolidation analysis were used.

Table 4: Soil parameters for the Soft Soil Creep model in the third analyse.

layer	γ [kN/m ³]	λ^* [-]	κ^* [-]	μ^* [-]	ν_{ur} [-]	ϕ'_{cs} [°]	k [10 ⁻¹⁰ m/s]
A1N	19.1	0.04	0.004	0.0013	0.15	34.0	10000
A1S	19.1	0.06	0.006	0.002	0.15	34.0	10
B1	17.3	0.115	0.0115	0.0038	0.15	26.0	5
B2	17.8	0.09	0.009	0.003	0.15	26.0	5
B3	16.7	0.115	0.0115	0.0038	0.15	26.0	5
B4/B5	20.0	0.05	0.005	0.0017	0.15	28.0	2
B7a	19.6	0.08	0.008	0.0027	0.15	27.0	5
B7b	17.8	0.11	0.011	0.0037	0.15	27.0	5
B8/B9/B10	19.0	0.08	0.008	0.0027	0.15	25.0	3

Table 5: Soil parameters for the Mohr-Coulomb model in the third analyse.

layer	γ [kN/m ³]	E [kPa]	ν [-]	ϕ [°]	c' [kPa]	ψ [°]	k [10 ⁻¹⁰ m/s]
MG	18.0	500	0.33	34.0	12.0	0.0	10000
A2	18.2	13700	0.33	34.0	0.0	0.0	10000
B6	19.1	11600	0.33	34.0	0.0	0.0	10000

Although the third analysis would seem to give realistic inclinations (Figure 18) and similarly a realistic average settlement, some details are still not satisfactorily modelled. These details refer to the loading of the tower by lead ingots as done from July 1993 up to January 1994. During this period a total load of 700 t was put on the north side of the foundation. Due to this loading the third consolidation analysis gives a northward change of inclination of 0.07°, whereas only 0.014° were measured. Similarly an additional average settlement of 8.8 mm was obtained, whereas the measurements gave only 2.5 mm. The measured response of the tower to the counterweight loading indicates that reloading (on the north side) was modelled much too soft. Two reasons for this should be mentioned. The first reason is that we have adopted an elastic unloading-reloading law with $K = p'/\kappa^*$, where K is the bulk modulus of the soil and p' the effective mean stress. Hence unloading-reloading moduli are proportional to stress level, which implies a very low soil stiffness just below the north side of the tower. In reality reloading stiffness is not fully linear on p' , and we overestimate the stress-level dependency especially at low stress levels.

Besides the stress-level, the soil stiffness is influenced by the strain-level. For small unload-reload cycles, soil is known to behave very stiff. For extremely small unload-reload cycles, being described by so-called small-strain stiffness, soil is even behaving extremely stiff. In order to improve the Pisa-model for unloading-reloading, we decided to decrease the swelling modulus κ^* , so that higher values of the elastic bulk modulus $K = p'/\kappa^*$ would result.

Fourth consolidation analysis

We decreased the swelling index of all clay and silt layers by 50 %. Hence, instead of using the rule $\kappa^* = \lambda^*/10$, we now consider $\kappa^* = \lambda^*/20$. Besides the swelling index, all parameters were taken conform the third analysis.

Computational results of the 4th consolidation analysis show that the effect of counterweight loading is indeed governed by the swelling index κ^* . Displacements due to the counterweights were found to be proportional to κ^* , as expected from a model with elastic compliances that are proportional to κ^* . However, in order to get a proper stiffness for the counterweight loading we do not advocate a simple reduction of κ^* , as done in the 4th consolidation analysis, as this would not improve the general performance of the model. Indeed, it can be observed from Figure 19 that the overall behaviour of the tower is better modelled with $\kappa^* = \lambda^*/10$ than with $\kappa^* = \lambda^*/20$.

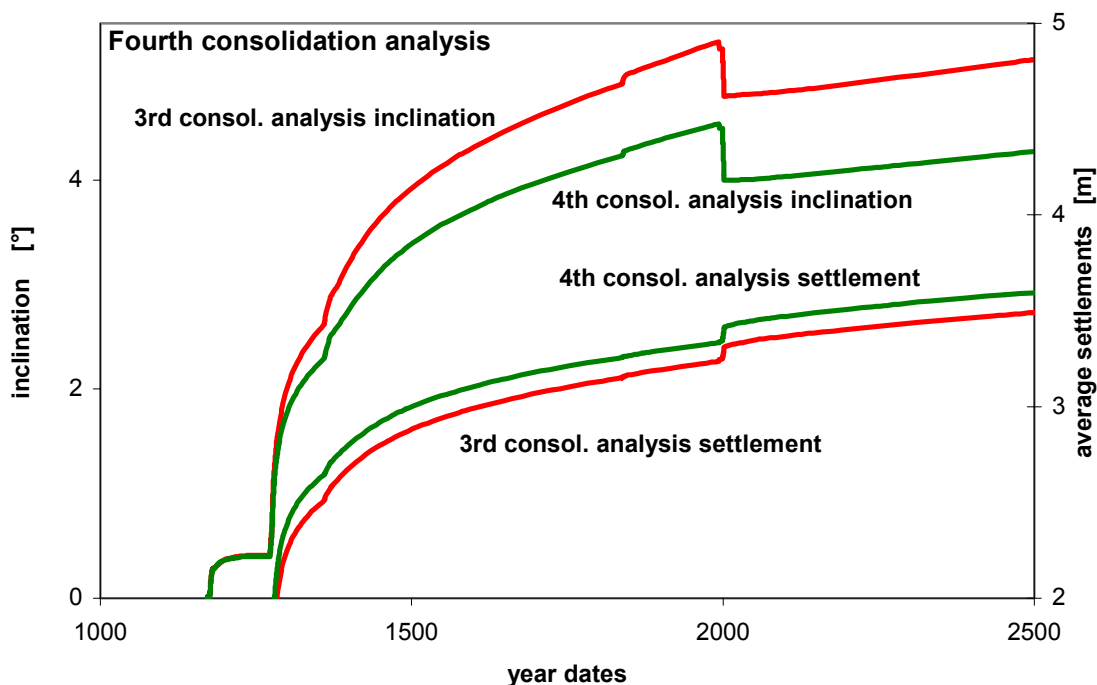


Figure 19: Influence of the swelling modulus κ^* on inclination and settlement.

This relates to the fact that we use an isotropic elasto-viscoplastic model in which plastic strain rates are co-axial to the current stress tensor and elastic strain rates are co-axial to rates of stress. On using a ratio of $\lambda^*/\kappa^* = 20$, one obtains a model in which plastic strains dominate elastic strains with a ratio of 19 over 1. As a consequence, total strains are nearly entirely plastic and thus nearly coaxial to the total stress tensors. This explains the relatively large average settlement and the relatively low inclination from the 4th consolidation analysis, being shown in Figure 19. Hence, the use of very large λ^*/κ^* -ratios is not advocated for use in the present Soft-Soil-Creep model. No doubt, this improves its performance in small unloading small reloading stages, but it deteriorates its performance in most other type of loadings. For a proper incorporation of the so-called small-strain stiffness, it would be necessary to modify the present isotropic elasto-viscoplastic model into a type of kinematic elasto-viscoplastic model with a small elastic nucleus.

7.2 Data from the 3rd Consolidation Analysis

First phase of construction from 1173 to 1178

The first construction phase of the tower from 1173 to 1178 was subdivided into five stages. Each stage was given a duration of exactly one year. During the first 35 days of such a year the tower height was increased, assuming no drainage at all, and during the rest of the year consolidation was modelled under constant load of the tower, using additional time steps. This scheme of undrained loading and subsequent consolidation was chosen, as the computer program did not allow for a combination of loading and consolidation in one and the same time step. In this way the foundation with a thickness of 3 m was modelled in exactly one year, i.e. the year 1173. Subsequently an additional height of 6 m was modelled in the year 1174, an extra height of again 6 m in 1175, etc. Finally the total height of 29 m above foundation level was achieved at the end of 1178.

Figure 20 shows the excess pore pressure distribution at the very end of the first construction phase, i.e. at the very end of 1178. Considering an average foundation

pressure of 323 kPa, the maximum excess pore pressure is found to be 74 kPa and the average settlement is computed to be 46 cm. The resulting inclination of 0.22° is still relatively small.

The first construction phase of 5 years is followed by a long construction pause up to the year 1272. During this period we applied the PLAXIS option of automatic time stepping. After a period of about 10 years, excess pore pressures appeared to have dissipated completely. Further deformations up to the year 1272 result from pure creep under constant effective stresses. At the end of this period the computed average settlement is 1.25 m and the computed inclination is 0.38° .

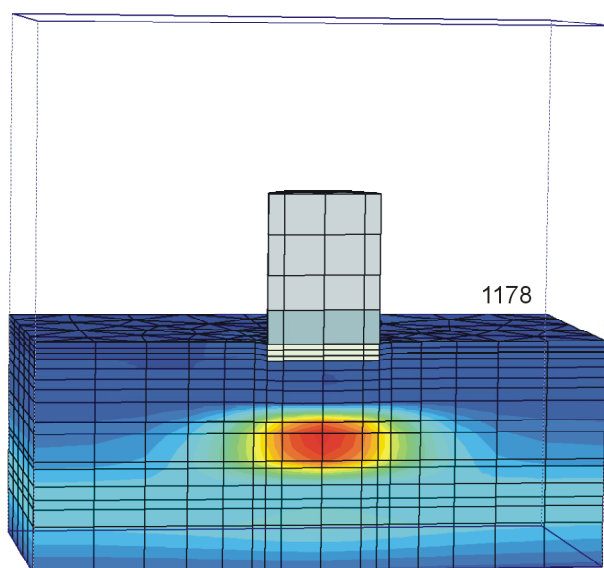


Figure 20: Excess pore pressure at the end of the first construction phase. The red zone has a maximum excess pore pressure of 74 kPa; the average settlement is 0.46 m; the inclination is 0.22° .

Second phase of construction from 1272 to 1278

The second phase of construction is modelled by subdividing this period in four stages. Each stage has a duration of 548 days, giving a total construction phase of $4 * 548$ days, i.e. 6 years starting in 1272. Each stage is modelled by an additional construction height of 5 m or 6 m, to obtain at the end a total tower height of 51 m (no bell chamber). Each *undrained* loading stage was applied in a period of 48 days followed by a consolidation period of 500 days. At the end of the second construction phase (end of 1278), excess pore pressures were computed to be 59 kPa, as indicated in Figure 21. At this stage the average foundation pressure is 473 kPa, the average settlement is 1.74 m and the inclination was computed to be 1.05° .

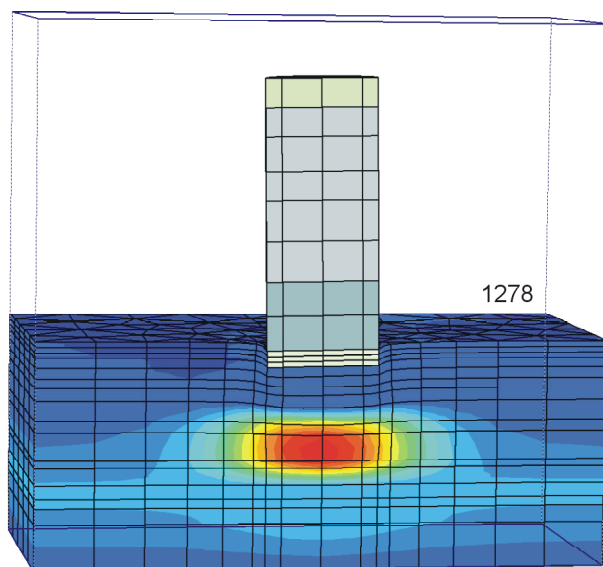


Figure 21: Excess pore pressure at the end of the second construction phase. The red zone has a maximum excess pore pressure of 59 kPa; the average settlement is 1.74 m; the inclination is 1.05° .

The second construction phase is followed by a long construction pause of 82 years up to 1360. As for the long first construction pause, the second one was modelled by using the automatic time-stepping procedure of the PLAXIS code. To cover this long construction pause a large number of additional time steps were applied, with consolidation in the beginning and creep under constant effective stresses for most of the time. At the end of this construction pause we computed an average settlement of 2.55 m and an inclination of 2.62°.

Third construction phase (bell chamber) from 1360 to 1370

Finally after the second construction pause (again approximately 100 years) the bell chamber was built during the years 1360-1370. The construction of the bell chamber is modelled in one single *undrained* loading stage of 52 days that is followed by a consolidation phase of 3600 days. Because of the small additional load and the long construction period only small excess pore pressures occur at the end of this period as shown in Figure 22. The red zone represents the highest excess pore pressure of only 3 kPa. At the end of construction in 1370 the average foundation pressure is 496 kPa, the average settlement is 2.60 m and the inclination of the tower is computed to be 2.81°.

From 1370 to 1838 excess pore pressures remained practically zero and the computer simulation showed a steadily increase of the inclination from 2.8° up to 4.6° due to creep. This effect of a long creep period is observed when comparing Figures 23a and 23b. These figures show an increase of the vertical stress σ_z' on the south side with progression of creep. The left picture shows the stress distribution σ_z' just after the construction of the bell chamber in 1370, whereas the right one reflects the stress distribution in the year 1838. Both pictures are plotted in the same scale. With progressing creep the vertical stresses increase in the south and decrease in the north.

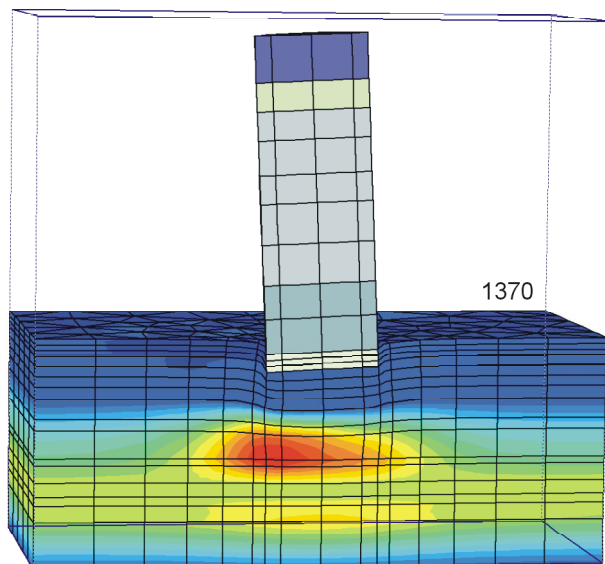


Figure 22: Excess pore pressures directly after the construction end of the bell chamber. The red zone has a maximum excess pore pressure of 3 kPa; the average settlement is 2.60 m; the inclination is 2.81°.

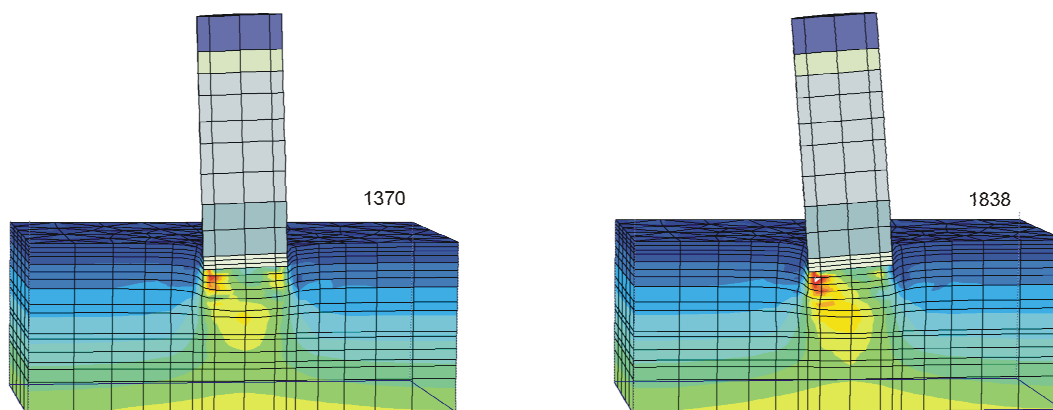


Figure 23: Vertical effective stress σ'_z before (left) and after (right) creep

Simulation of Catino excavation

The excavation of the Catino was modelled by removing elements around the foundation of the tower. At the south side this was done to a depth of 2 m and at the north side only 1 m was excavated. Figure 24 shows relevant details of the mesh around the foundation. The Catino-elements were partly removed in an undrained phase with a duration of 30 days followed by a consolidation period of 1 year. The excavation was completed in another undrained phase of 30 days, being followed by a long period with significant creep up to 1993. Considering the development of the inclination as a function of time (Figure 18), it would seem that the Catino has caused an extra inclination of about 0.4° . This influence of the Catino on the inclination is most likely related to the rotation stiffness of the tower (Jamiolkowski, 1999). Considering the analogy of an *inverted pendulum* (Jamiolkowski, 1999), it is logical that a deletion of shear stresses at the vertical sides of the foundation will reduce the rotation stiffness of the tower.

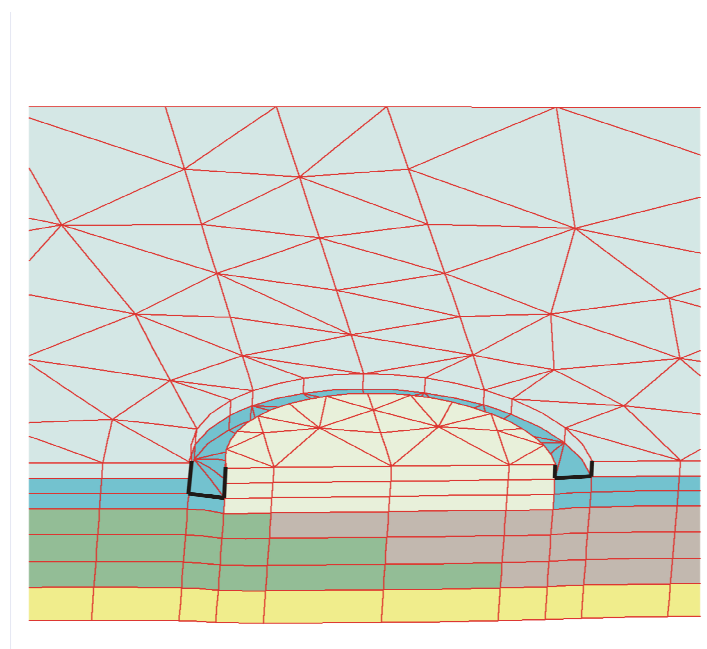


Figure 24: Detail of FE mesh around the foundation of the tower to show the modelling of the Catino simulation.

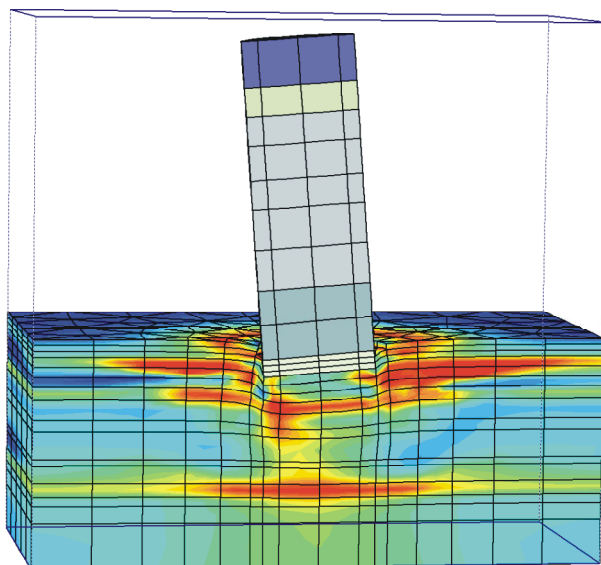


Figure 25: Relative shear shadings in the year 1993.

Figure 25 represents a true scale geometry of the tower in the year 1993. The computed inclination is 5.02° and the average settlement is 3.22 m. Due to the excavation of the Catino the settlements have also increased from 3.12 m up to 3.22 m. The red colour in Figure 25 represents an area where the shear strength of the subsoil is completely exhausted. This typically happens in the relative stiff sand layers. The large deformations of the silt layer also create zones in a fully plastic state of stress.

7.3 Counterweights, Soil Extraction and Future Creep

Simulation of counterweight loads

The placement of the lead ingots from July 1993 to January 1994 on the north side of the tower was modelled by adding an eccentric external load of 700 t. This was done by undrained loading over a period of 276 days and subsequent consolidation.

Simulation of soil extraction

The soil extraction has been simulated by reducing the volume of finite elements at the north side underneath the foundation. The shaded volume in Figure 26 indicates elements with a total volume reduction of 6.8 m³ in 1999 (over a period of 122 days) and an additional reduction of 18.2 m³ in 2000 (during a period of 549 days). The total amount of 25 m³ was taken to realise a backward rotation of 0.476° and an additional settlement of 6.0 cm. In reality the excavation was much more located to the east and west sides of the tower and this may also explain the fact that the numerical extraction is well below the real amount of extracted volume.

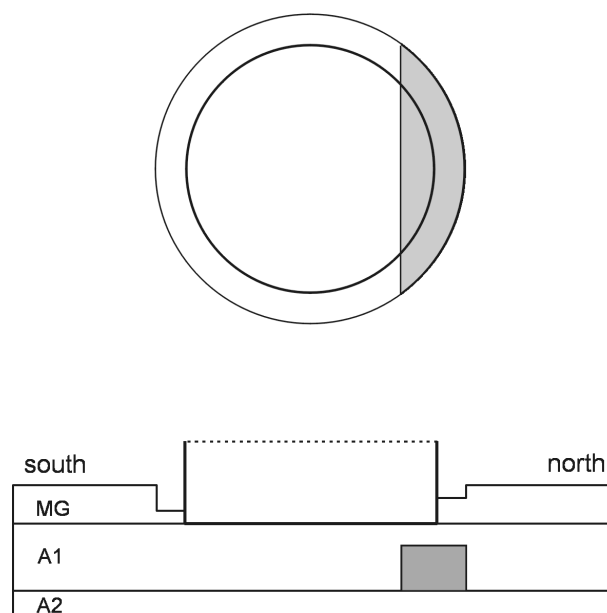


Figure 26: Soil extraction under the tower foundation. The shaded regions mark clusters of numerical uniform soil extraction.

Future creep

Finally after soil extraction, the Plaxis time-stepping procedure was used to predict further tower movements up to the year 2500. This stage of simulation showed an

extremely slow increase of the inclination and similarly a slow increase of average settlements. As shown in Figure 27, all movements are roughly linear with time when considering coming centuries.

Table 6: Computed future creep rates

	rate of rotation [degrees/century]	rate of settlement [cm/century]
drained analysis	0.11	4.6
1 st consolidation analysis	0.17	5.8
3 rd consolidation analysis	0.06	3.7

The difference between the data from the 1st consolidation analysis and the 3rd consolidation analysis is significant. In comparison to the 1st consolidation analysis deformation rates are lower in the 3rd consolidation analysis. This relates to the calibration of the soil parameters. In the 3rd consolidation analysis the creep index and the modified compression index are smaller than those in the 1st consolidation analysis and this explains the differences. We consider the 3rd consolidation analysis most realistic, but somewhat larger creep rates as indicated by results from the 1st analysis should not be entirely excluded.

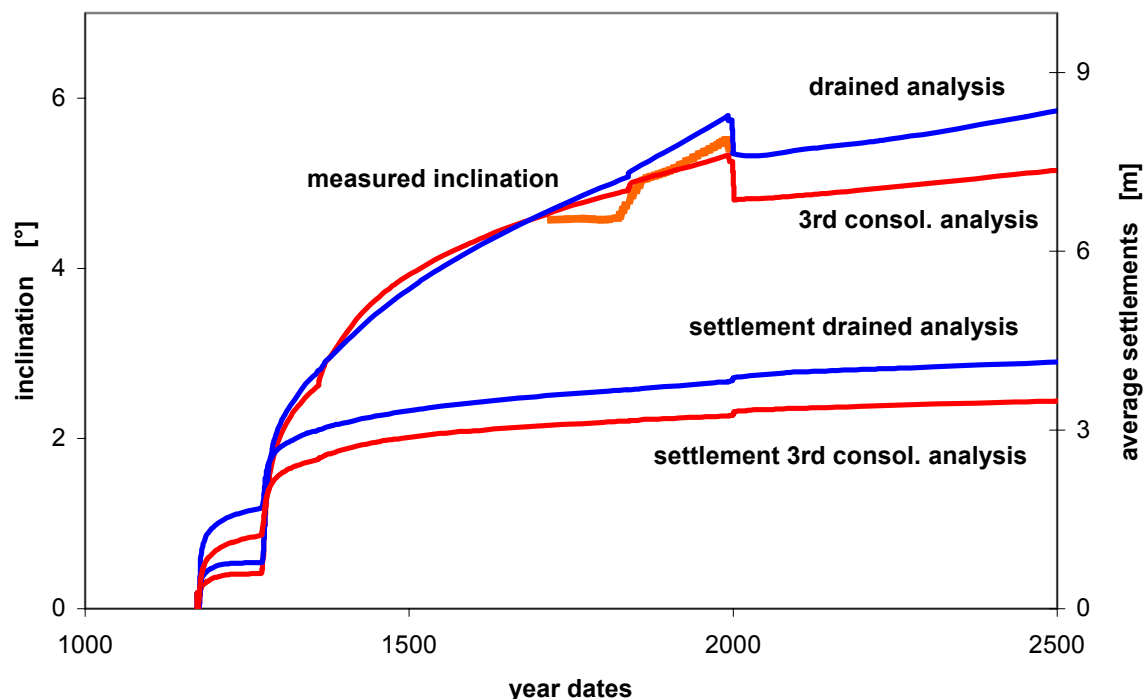


Figure 27: Comparison between drained and consolidation analysis

8 Conclusions

On using existing soil data on the Pisa site and in particular the ones by Calabresi (1996), the current situation can be back-analysed extremely well. For triggering the tilting of the tower, we have used a moderate stiffness difference within the silty soil layer A1 directly underneath the tower. The tilting of the tower is straightforwardly obtained when using the Soft-Soil-Creep model to account for material non-linearity in combination with an updated Lagrange method that accounts for geometric non-linearity. Similarly a very realistic settlement is obtained.

In addition to the Soft-Soil-Creep model we have used a rate independent model, named the Soft-Soil model. This model resembles the creep model in many ways and uses basically the same input parameters as the creep model, but it obviously does not

incorporate creep effects. On using this model in combination with parameters of the creep model, we underestimate deformations considerably.

The computational results indicate that the soil extraction was really necessary, as the computations show a relatively high creep rate before extraction. After the extraction this creep rate is considerably reduced. For the coming period of a hundred years we expect hardly any increase of the inclination. Considering our results it will take at least another 500 years before the tower will reach the pre-extraction inclination again.

9 Literature

A.G.I. (1991), *The leaning tower of Pisa – Present situation*, In A.G.I. (Eds.) Proceedings of the 10th ECSMFE, Volume 4: 1437-144, Florence, A.A. Balkema

A.G.I. (1991), *Pisa, Bell tower*, In A.G.I. (Eds.), Proceedings of the 10th ECSMFE, The contribution of geotechnical engineering to the preservation of Italian historic sites: 105-108, Florence

Berardi, G., Caroti, L., Giunta, G., Jamiolkowski, M. & Lancellotta, R. (1991), *Mechanical properties of Upper Pisa Clay*, In A.G.I. (Eds.), Proceedings of the 10th ECSMFE, Volume 1: 7-10, Florence, A.A. Balkema

Brinkgreve, R.B.J. & Vermeer, P.A. (Eds.) (1998), PLAXIS Finite Element Code for Soil and Rock Analyses, Version 7, A.A. Balkema

Brinkgreve, R.B.J. & Vermeer, P.A., (Eds.) (2001), PLAXIS Finite Element Code for Soil and Rock Analyses **3D Tunnel**, Version 1, A.A. Balkema

Burland, J.B. (1965), *The yielding and dilation of clay*, (Correspondence), Géotechnique Volume 115: 211-214

Burland, J.B. (1967), *Deformation of soft clay*, Dissertation, Cambridge University

Burland, J.B. & Potts, D.M. (1994), *Development and application of a numerical model for the leaning tower of Pisa*, In Shibuya, S., Mitachi, T. & Miura, S. (Eds.), Proceedings of 1st Int. Conf. on Pre-failure Deformation of Geomaterials, Volume 2: 715-738, Sapporo, A.A. Balkema

Calabresi, G., Callisto L. and Rampello S. (1994), *Rapporto di sintesi delle prove eseguite sui campioni del sottosuolo della Torre di Pisa, prelevati dal sondaggio L2*. Internal Report, Università degli studi di Roma "La Sapienza", Dipartimento di Ingegneria Strutturale e Geotecnica.

Calabresi G., Rampello S. and Callisto L. (1993), *The Leaning Tower of Pisa: Geotechnical Characterisation of the Tower's Subsoil within the Framework of Critical State Theory*, Università degli studi di Roma "La Sapienza", Dipartimento di Ingegneria Strutturale e Geotecnica, Studi e Ricerche 1/93-2/93

Calabresi, G., Rampello, S., Callisto, L. & Viggiani, G.M.B. (1996), *The Leaning Tower of Pisa – Soil parameters for the numerical modelling of the tower resulting from the most recent investigations*, Laboratorio geotecnica Dipartimento di Ingegneria Strutturale Geotecnica, Università di Roma "La Sapienza"

Jamiolkowski, M., (coordinator) (1999), *Workshop on the Pisa Tower "The Restoration of the Leaning Tower: Present Situation and Perspectives"*. Pre-prints of the Reports Volume 1

Janbu, N. (1969), *The resistance concept applied to soils*, In Proceedings of the 7th ICSMFE Volume 1:191-196, New Mexico

Lancellotta R. and Pepe C. (1990), *Pisa Tower – A preliminary report*, Internal Reports Ns. 2.1-2.2-2.3, Politecnico di Torino, Dipartimento di Ingegneria Strutturale

Potts, D.M. (1993), *Calibrazione di un modello geotecnico agli elementi finiti e valutazione degli effetti indotti a seguito di alcuni interventi di consolidamento della torre di Pisa*, GCG Computing London UK

Potts, D.M. & Burland, J.B. (2000), *Development and application of a numerical model for simulating the stabilisation of the leaning tower of Pisa*, In Smith, D.W. & Carter, J.R. (Eds.), Proceedings of the John Booker Memorial Symposium Developments in Theoretical Geomechanics: 737-757, Sydney, A.A. Balkema

Stolle D.F.E., Bonnier, P.G. & Vermeer, P.A. (1997), *A soft soil model and experiences with two integration schemes*, In Pande, G.N. & Pietruszczak, S. (Eds.), Proceedings of the 6th NUMOG: 123-128, Montreal, A.A. Balkema

Vermeer, P.A., Stolle, D.F.E. & Bonnier, P.G. (1997), *From the classical theory of secondary compression to modern creep*, In Yuan, J.-X. (Ed.), Proceedings of the 9th IACMAG Volume 4: 2469-2478, Wuhan, A.A. Balkema

Vermeer, P.A. & Neher, H.P. (1999), *A soft soil model that accounts for creep*, In Bringreave, R.B.J. (Ed.), Proceedings of the Int. Symposium "Beyond 2000 in Computational Geotechnics": 249-261, Amsterdam, A.A. Balkema